

# Dynamics of gravitating magnetic monopoles

Nobuyuki Sakai\*

*Department of Physics, Waseda University, Shinjuku-ku, Tokyo 169, Japan*

(Revised 9 March 1996)

## Abstract

According to previous work on magnetic monopoles, static regular solutions are nonexistent if the vacuum expectation value of the Higgs field  $\eta$  is larger than a critical value  $\eta_{\text{cr}}$ , which is of the order of the Planck mass. In order to understand the properties of monopoles for  $\eta > \eta_{\text{cr}}$ , we investigate their dynamics numerically. If  $\eta$  is large enough ( $\gg \eta_{\text{cr}}$ ), a monopole expands exponentially and a wormhole structure appears around it, regardless of coupling constants and initial configuration. If  $\eta$  is around  $\eta_{\text{cr}}$ , there are three types of solutions, depending on coupling constants and initial configuration: a monopole either expands as stated above, collapses into a black hole, or comes to take a stable configuration.

To appear in *Physical Review D*

---

\*Electronic address: sakai@cfi.waseda.ac.jp

## I. INTRODUCTION

In recent years static and spherically symmetric solutions of the Einstein-Yang-Mills-Higgs system have been intensively studied in the literature [1–3]. One purpose of such investigation has been to understand the nature of black holes, especially in the context of the no-hair conjecture; it was shown that non-trivial black holes are stable and hence the monopole black hole could be one of the most plausible counterexamples. The other interest has been in the properties of particle-like solutions; it was shown that such regular monopoles exist only if the vacuum expectation value of the Higgs field  $\eta$  is less than a critical value  $\eta_{\text{cr}}$ , which is of the order of the Planck mass  $m_{\text{Pl}}$ . This result naturally gives rise to the next question: what is the fate of monopoles for  $\eta > \eta_{\text{cr}}$ ?

Because the only static solution for  $\eta > \eta_{\text{cr}}$  is the Reissner-Nordström black hole, we can expect that a monopole which is regular initially evolves into the Reissner-Nordström black hole. Even if this speculation is reasonable, we still do not know how the black hole formation occurs. One could imagine two alternatives: a monopole just shrinks, or its core continues to expand inside the black-hole horizon, just as a “child universe” [4].

Linde and Vilenkin independently pointed out the latter possibility in the context of the “topological inflation” model [5]. They claimed monopoles as well as other topological defects expand exponentially if  $\eta > O(m_{\text{Pl}})$ . Their discussions for the Einstein-Higgs system were verified by our numerical simulation in [6]: we found that domain walls and global monopoles inflate if and only if  $\eta \gtrsim 0.33m_{\text{Pl}}$ . The next question on this monopole inflation is similarly what happens to magnetic monopoles in the Einstein-Yang-Mills-Higgs system. Because we cannot find an answer to the question only by analyzing static solutions, we investigate dynamic monopole solutions in this paper.

The plan of this paper is as follows. In Sec. II, we derive the basic equations and explain how we solve those dynamical equations numerically. In Sec. III, we offer analytic discussions and numerical results. Sec. IV is devoted to summary and discussions. In this paper we use the units  $c = \hbar = 1$ .

## II. BASIC EQUATIONS

The  $SO(3)$  Einstein-Yang-Mills-Higgs system is described by

$$S = \int d^4x \sqrt{-g} \left[ \frac{m_{\text{Pl}}^2}{16\pi} \mathcal{R} - \frac{1}{4} (F_{\mu\nu}^a)^2 - \frac{1}{2} (D_\mu \Phi^a)^2 - V(\Phi) \right], \quad (2.1)$$

with

$$V(\Phi) = \frac{1}{4} \lambda (\Phi^2 - \eta^2)^2, \quad \Phi \equiv \sqrt{\Phi^a \Phi^a}, \quad (2.2)$$

$$F_{\mu\nu}^a \equiv \partial_\mu A_\nu^a - \partial_\nu A_\mu^a + e\epsilon^{abc}A_\mu^b A_\nu^c, \quad D_\mu \Phi^a \equiv \nabla_\mu \Phi^a + e\epsilon^{abc}A_\mu^b \Phi^c, \quad (2.3)$$

where  $A_\mu^a$  and  $F_{\mu\nu}^a$  are the  $SU(2)$  Yang-Mills field potential and its field strength, respectively.  $\Phi^a$  is the real triplet Higgs field and  $V(\Phi)$  is its potential.  $\lambda$  and  $e$  are the Higgs self coupling constant and the gauge coupling constant, respectively.  $\nabla_\mu$  and  $D_\mu$  are the spacetime covariant derivative and the totally covariant derivative, respectively. The variation of (2.1) with respect to  $g_{\mu\nu}$ ,  $\Phi^a$  and  $A_i^a$  yield the Einstein equations,

$$G_{\mu\nu} \equiv \mathcal{R}_{\mu\nu} - \frac{1}{2}g_{\mu\nu}\mathcal{R} = \frac{8\pi}{m_{\text{Pl}}^2}T_{\mu\nu},$$

$$T_{\mu\nu} \equiv D_\mu \Phi^a D_\nu \Phi^a - g_{\mu\nu} \left[ \frac{1}{2}(D_\sigma \Phi^a)^2 + V(\Phi) \right] + F_{\mu\lambda}^a F_\nu^{a\lambda} - \frac{1}{4}g_{\mu\nu}(F_{\lambda\sigma}^a)^2, \quad (2.4)$$

and the equations for the matter fields,

$$D_\mu D^\mu \Phi^a = \frac{\partial V(\Phi)}{\partial \Phi^a}, \quad (2.5)$$

$$D_\mu F^{a\mu\nu} = -e\epsilon^{abc}\Phi^b D^\nu \Phi^c. \quad (2.6)$$

We assume a spherically symmetric spacetime and adopt the coordinate system,

$$ds^2 = -dt^2 + A^2(t, r)dr^2 + B^2(t, r)r^2(d\theta^2 + \sin^2\theta d\varphi^2). \quad (2.7)$$

For the matter fields, we adapt the 't Hooft-Polyakov ansatz in such a way that we can apply it to a time-dependent curved spacetime:

$$\Phi^a = \Phi(t, r)\hat{r}^a, \quad \hat{r}^a \equiv (\sin\theta \cos\varphi, \sin\theta \sin\varphi, \cos\theta). \quad (2.8)$$

$$A_\mu^a = \frac{\partial(\sqrt{g_{\theta\theta}}\hat{r}^b)}{\partial x^\mu} \epsilon^{abc}\hat{r}^c \frac{1-w(t, r)}{e\sqrt{g_{\theta\theta}}}. \quad (2.9)$$

With the metric (2.7) and the 't Hooft-Polyakov ansatz (2.8) and (2.9), we write down the field equations (2.4)-(2.6) as

$$-G_0^0 \equiv K_2^2(2K - 3K_2^2) - \frac{2B''}{A^2B} - \frac{B'^2}{A^2B^2} + \frac{2A'B'}{A^3B} - \frac{6B'}{A^2Br} + \frac{2A'}{A^3r} - \frac{1}{A^2r^2} + \frac{1}{B^2r^2}$$

$$= \frac{8\pi}{m_{\text{Pl}}^2} \left[ \frac{\dot{\Phi}^2}{2} + \frac{\Phi'^2}{2A^2} + \left(\frac{w\Phi}{Br}\right)^2 + V + \frac{1}{(eBr)^2} \left\{ \dot{w}^2 + \frac{w'^2}{A^2} + \frac{1}{2}\left(\frac{w^2-1}{Br}\right)^2 \right\} \right], \quad (2.10)$$

$$\frac{1}{2}G_{01} \equiv K_2^{2'} + \left(\frac{B'}{B} + \frac{1}{r}\right)(3K_2^2 - K) = \frac{4\pi}{m_{\text{Pl}}^2} \left[ \dot{\Phi}\Phi' + \frac{2\dot{w}w'}{(eBr)^2} \right], \quad (2.11)$$

$$\frac{1}{2}(G_1^1 + G_2^2 + G_3^3 - G_0^0) \equiv \dot{K} - (K_1^1)^2 - 2(K_2^2)^2$$

$$= \frac{8\pi}{m_{\text{Pl}}^2} \left[ \dot{\Phi}^2 - V + \frac{1}{(eBr)^2} \left\{ \dot{w}^2 + \frac{w'^2}{A^2} + \frac{1}{2} \left( \frac{w^2 - 1}{Br} \right) \right\} \right], \quad (2.12)$$

$$\ddot{\Phi} - K\dot{\Phi} - \frac{\Phi''}{A^2} - \left( -\frac{A'}{A} + \frac{2B'}{B} + \frac{2}{r} \right) \frac{\Phi'}{A^2} + \frac{2w^2\Phi}{B^2r^2} + \frac{dV}{d\Phi} = 0, \quad (2.13)$$

$$\ddot{w} - K_1^1\dot{w} - \frac{w''}{A^2} + \frac{A'w'}{A^3} - \frac{w(1-w^2)}{B^2r^2} + e^2\Phi^2w = 0, \quad (2.14)$$

where the overdot and the prime denote the partial derivative with respect to  $t$  and  $r$ , respectively. We have introduced the extrinsic curvature tensor of a  $t = \text{constant}$  hypersurface,  $K_{ij}$ , whose components are given by

$$K_1^1 = -\frac{\dot{A}}{A}, \quad K_2^2 (= K_3^3) = -\frac{\dot{B}}{B}, \quad (2.15)$$

and we have denoted its trace by  $K \equiv K_i^i$ .

As an initial configuration of the matter fields, we adopt the functional form of the static solution in a flat spacetime with  $\lambda = 0$ :

$$\begin{aligned} \Phi(t=0, r) &= \Phi_{\text{flat}}\left(\frac{r}{c_\Phi}\right) \equiv \eta \left[ \frac{1}{\tanh(e\eta r/c_\Phi)} - \frac{1}{e\eta r/c_\Phi} \right], \\ w(t=0, r) &= w_{\text{flat}}\left(\frac{r}{c_w}\right) \equiv \frac{e\eta r/c_w}{\sinh(e\eta r/c_w)}, \end{aligned} \quad (2.16)$$

where  $c_\Phi$  and  $c_w$  are the initial size parameters. The configurations of  $\Phi_{\text{flat}}(r)$  and of  $w_{\text{flat}}(r)$  are illustrated in Fig. 1. As to the time-derivative, we suppose  $\dot{\Phi}(t=0, r) = \dot{w}(t=0, r) = 0$ . In order to set up consistent initial data, we have to solve the constraint equations (2.10) and (2.11). At this point, there are four unknown variables,  $A$ ,  $B$ ,  $K$  and  $K_2^2$ , in the two constraint equations; two of the variables are arbitrarily chosen. One of the methods which is usually adopted is to assume  $K = \text{const}$  and  $A = B$ . In this system, however, the condition of  $K = \text{const} \neq 0$  is not appropriate because the far region is asymptotically flat. Further, in the range where there exists no static solution, we cannot fix  $K = 0$  even momentarily. As an alternative, thereby, we suppose  $A(t=0, r) = B(t=0, r) = 1$  and solve the constraint equations (2.10) and (2.11) to determine  $K(t=0, r)$  and  $K_2^2(t=0, r)$ . This treatment is suitable for this system because we obtain

$$-\frac{K}{3} \approx -K_2^2 \approx \sqrt{\frac{8\pi}{3m_{\text{Pl}}^2} \left( \frac{\Phi'^2}{2} + \frac{\Phi^2}{r^2} + V \right)}, \quad (2.17)$$

which approaches zero as  $r$  increases; we can construct an asymptotically flat spacetime without iterative integration. We have also assumed  $K(t=0, r) < 0$ : every point in

the spacetime is locally expanding. The numerical boundary is fixed at  $r = 30/(e\eta)^{-1}$  or  $60/(e\eta)^{-1}$ .

In order to solve the dynamical equations, we use a finite difference method with 2000 to 10,000 meshes. Now we have six dynamical variables:  $A$ ,  $B$ ,  $K$ ,  $K_2^2$ ,  $\Phi$  and  $w$ . Equations (2.12)-(2.15) provide the next time-step of  $A$ ,  $B$ ,  $K$ ,  $\Phi$  and  $w$ , respectively. At each step, we integrate (2.11) in the  $r$ -direction to obtain  $K_2^2$ . In this way we have reduced spatial derivatives appearing in the equations, which may become seeds for numerical instability. The Hamiltonian constraint equation (2.10) remains unsolved during the evolution and is used for checking numerical accuracy. We stop numerical computation when some errors exceed a few percent.

In order to understand the spacetime structure from the numerical data, it is useful to observe the signs of the expansion of a null geodesic congruence. Nambu and Siino [7] also utilized this tool to study wormhole formation in a singlet scalar field system. For the metric (2.7), the expansion  $\Theta_{\pm}$  is written as

$$\Theta_{\pm} = k_{\pm;2}^2 + k_{\pm;3}^3 = 2 \left[ -K_2^2 \pm \frac{(Br)'}{ABr} \right], \quad (2.18)$$

where  $k_{\pm}^{\mu} = (-1, \pm A^{-1}, 0, 0)$  is an outgoing (+) or ingoing (−) null vector. We observe the signs of  $\Theta_{\pm}$  at all points in the numerical spacetime. For later convenience, we define “RI” as the region where both  $\Theta^+$  and  $\Theta^-$  are positive, and “RII” as the region where they are negative. We can interpret that the region around RI is de Sitter-like and the region around RII is Schwarzschild-like. The two-surface which bounds RI or RII is called an “apparent horizon”. Later, we will use the term “black hole horizon” to refer to any boundary of RII. And, we will use the term “cosmological horizon” in the sense that no information beyond it reaches the center of a monopole; only the innermost boundary of RI is called the cosmological horizon.

### III. NUMERICAL RESULTS

Before we move on to numerical simulation, we offer a rough discussion on the effect of the gauge fields on the gravitational field. In our previous paper [6], we investigated the effect for static monopole solutions and found that the gauge fields generate an attractive force. This property is also described in the time-dependent coordinate system (2.7) as follows.

In a homogeneous and isotropic spacetime, the evolution of the scale factor  $a(t)$  follows

$$\frac{3\ddot{a}}{a} = -\frac{4\pi}{m_{\text{Pl}}^2}(\rho + 3p), \quad (3.1)$$

where  $\rho$  and  $p$  are the energy density and the pressure of a matter, respectively. Equation (3.1) indicates that the sign of  $\rho + 3p$  determines whether the acceleration of the cosmic

expansion is positive or negative. We can extend this discussion to general spacetimes: the sign of  $\rho + \Sigma p_i \equiv -T_0^0 + T_i^i$  determines whether a local region expands with positive acceleration or not. A corresponding equation in the present system to (3.1) is (2.12). At the origin, (2.12) reduces to

$$\frac{3\ddot{A}}{A}\Big|_{r=0} = -\frac{4\pi}{m_{\text{Pl}}^2}(\rho + \Sigma p_i)_{r=0} \equiv -\frac{4\pi}{m_{\text{Pl}}^2}\left(-2V + \frac{3w''^2}{e^2 A^4}\right)_{r=0} \quad (3.2)$$

In the case of global monopoles, the second term of the right-hand side disappears, and hence the central region is always locally de Sitter spacetime. If gauge fields exist, however, the local acceleration at the center also depends on the second term. Although the exact value of  $\partial^2 w / (A\partial r)^2$  cannot be determined without solving the full dynamical equations, we can estimate its order by use of the static solution in a flat spacetime with  $\lambda = 0$ . Assuming  $\partial^2 w / (A\partial r)^2 = b w''_{\text{flat}}(r)$  with  $b = O(1)$ , we have

$$\rho + \Sigma p_i|_{r=0} = \frac{e^2 \eta^4}{4} \left(-\frac{\lambda}{e^2} + \frac{2}{3}b\right), \quad (3.3)$$

which lets us understand how the local expansion of the spacetime in the center depends on  $\lambda/e^2$ . We see that, if  $\lambda/e^2 \ll 1$ , the monopole core is an attractive spacetime; while, if  $\lambda/e^2 \gg 1$ , it is repulsive like de Sitter spacetime. Of course, if the initial configuration is quite different from that of the static solutions, i.e.,  $b \neq O(1)$ , the above discussion is not true. The dynamics may also depend on initial configuration.

In what follows, by use of the method in Sec. II, we will numerically integrate the field equations (2.10)-(2.14). To show the results, we define  $X$  as a proper distance in the radial direction:  $X \equiv \int_0^r A dr$ . We also define the boundaries of a monopole in two ways:  $X_\Phi(t) = X$  at the position of  $\Phi = \eta/2$  and  $X_w(t) = X$  at the position of  $w = 1/2$ . We normalize time and length by the horizon scale defined as  $H_0^{-1} \equiv (8\pi V(0)/3m_{\text{Pl}}^2)^{-\frac{1}{2}}$ .

First, we check our numerical code by solving the equations for the case of weak gravity. In Fig. 2 we set  $\eta = 0.1m_{\text{Pl}}$  and  $\lambda/e^2 = 0.1$ , and give two initial configurations:  $c_\Phi = c_w = 1$  and 0.5. We plot the trajectories of  $X_\Phi(t)$ . We find that the fields behaves stably; this reasonable result indicates that our numerical code works well.

From now on, we concentrate on the parameter range where no static solution exists. In Fig. 3 we set  $\eta = 0.4m_{\text{Pl}}$  and  $\lambda/e^2 = 0.1$ , and give two initial configurations:  $c_\Phi = c_w = 1$  in (a) and  $c_\Phi = c_w = 10$  in (b). In Fig. 3(a)(b) we plot the trajectories of  $X_\Phi(t)$  and  $X_w(t)$  as well as apparent horizons. The dynamics in these two cases contrast sharply: in (a) a monopole shrinks and black-hole horizons appear, while in (b) a cosmological horizon exists from the beginning and a monopole continues to expand. We also draw the distributions of  $\rho + \Sigma p_i$  in (c) and in (d), which correspond to the results in (a) and in (b), respectively. In (c) the values around the center become negative at the beginning, but they bounce back to positive values, which confirms that the monopole core never inflates. On the other hand,

in (d) the values of  $\rho + \Sigma p_i$  around the center remain negative from the beginning. This behavior indicates that exponential expansion really occurs inside the monopole. These two results tell us that monopoles for  $\eta > \eta_{\text{cr}}$  tend to be dynamic, and their dynamics depends on the initial configuration, contrary to the case of global monopoles.

As we will see soon, for larger  $\eta$ , monopoles are more likely to inflate rather than shrink. We show an example for larger  $\eta$  in Fig. 4; we set  $\eta = 0.55m_{\text{Pl}}$ ,  $\lambda/e^2 = 0.1$  and  $c_\Phi = c_w = 1$ . In Fig. 4(a) we plot the trajectories of  $X_\Phi(t)$  and  $X_w(t)$  as well as apparent horizons. (Please also refer to Fig. 5, which is a schematic sketch of the spacetime structure.) From the beginning there are two apparent horizons,  $S1$  and  $S2$ :  $S1$  is the cosmological horizon. Later other two apparent horizons,  $S3$  and  $S4$ , appear, and then  $S2$  and  $S4$  approach each other. These surfaces turn out to be black-hole horizons,  $S2'$  and  $S4'$ , the moment they intersect. In Fig. 4(b) we draw the distributions of  $\rho + \Sigma p_i$ . Contrary to the case of the contracting monopole in Fig. 3(a), the values around the center are initially positive, but they become negative. This suggests that, if  $\eta$  is large enough, a monopole begins to expand exponentially even if its initial size is not so large. We also show in Fig. 4(c) the relation between the proper distance along the radial direction and the circumference radius, which indicates a wormhole structure really appears. Figure 4 lets us understand how the wormhole is created. Because the expanding core is causally disconnected from the outer region, such an isolated region is called a “child universe”.

One may think that if  $\eta > \eta_{\text{cr}}$ , a monopole either expands or collapses, as shown in Fig. 3 or 4. However, we find some cases where a monopole neither expands nor collapses. An example of such solutions is shown in Fig. 6 ( $\eta = 0.3m_{\text{Pl}}$  and  $\lambda/e^2 = 1$ ). Setting  $c_\Phi = c_w = 1$ , we show the evolution of  $\Phi$  in (a) and that of  $w$  in (b), and the trajectories of  $X_\Phi(t)$  and of  $X_w(t)$  in (c). Although some oscillations remain outside the monopole, the core of the monopole approaches a stable configuration. We change the initial size in Fig. 6(d), finding monopoles with any initial size behave stably. These results indicate that there exist stationary solutions.

In order to see if such stable monopoles are really created in an expanding universe, we consider a different type of initial configurations: to give a small perturbation on the symmetric state (de Sitter spacetime). Specifically, we adopt a form,

$$\Phi(t = 0, r) = d \frac{r}{c} \exp\left[-\left(\frac{r}{c}\right)^2\right], \quad w(t = 0, r) = 1, \quad (3.4)$$

where we fix  $d = 0.1$  and  $c = 20$  in our analysis. In this way we see how a monopole configuration is formed from the nearly symmetric state. We assume  $\lambda/e^2 = 10$  and  $\eta/m_{\text{Pl}} = 0.3$ , as is the case in Fig. 6. Figure 7 shows that, once a monopole configuration is formed, it approaches a stable configuration instead of continuing to expand. This result supports the existence of stationary solutions. The existence of such solutions looks surprising, because one may expect that all solutions in the parameter range where no static solution exists must be dynamical. The existence of “stationary” solutions, however, does not contradict

the nonexistence of “static” solutions: the solutions in Figs. 6 and 7 cannot be described with a static coordinate system because the size of the monopole is greater than the cosmological horizon.

Finally we systematically survey the dynamics of monopoles for  $0.05 \leq \eta/m_{\text{Pl}} \leq 0.55$  and  $0.1 \leq \lambda/e^2 \leq 10$  and summarize the solutions in the  $\lambda/e^2$ - $\eta/m_{\text{Pl}}$  plane of Fig. 7. A square denotes a stable solution, as is the case in Fig. 2 or 6. A cross denotes the case where a monopole shrinks, as is the case in Fig. 3(a). A circle denotes the case where a monopole inflates and the wormhole structure appears, as is the case in Fig. 4. A dotted line indicates the maximum values of  $\eta/m_{\text{Pl}}$  versus  $\lambda/e^2$ , depicted approximately by use of Fig.6 in [1]. We vary  $c_{\Phi}$  and  $c_w$  from 1 to 10, and hence some parameter points are labeled as two symbols. We interpret these results as follows. In the case of  $\lambda/e^2 > 1$ , a monopole expands exponentially if  $\eta \gtrsim 0.35m_{\text{Pl}}$ ; this critical value has little dependence on  $\lambda/e^2$  and initial configuration, and almost agrees with that for global monopoles [6]. This agreement is quite reasonable because the effect of the gauge fields is smaller as  $\lambda/e^2$  is larger. Below the critical value, a monopole tends to take a stable configuration even in the theories where static solutions are nonexistent. In the case of  $\lambda/e^2 < 1$ , the dynamics also depend on  $\lambda/e^2$  and initial configuration. In some cases the effect of the gauge fields becomes dominant and a monopole shrinks and becomes a black hole. These results are consistent with our analytic discussions at the beginning of this section.

#### IV. SUMMARY AND DISCUSSIONS

We have studied the dynamics of magnetic monopoles numerically. Our main purpose has been to understand the behavior of monopoles in the case where static solutions are nonexistent.

If  $\eta$  is large enough ( $\gg \eta_{\text{cr}}$ ), a monopole inflates and a wormhole structure appears around it. We have shown how the wormhole connected with a child universe is created. We should emphasize that a child universe can be generated without fine-tuned initial conditions in this model, contrary to the case of a trapped false vacuum bubble [4]. In the case of  $\lambda/e^2 > 1$ , the condition of inflation is  $\eta \gtrsim 0.35m_{\text{Pl}}$ , which has little dependence on  $\lambda/e^2$  and initial configuration. Below the critical value, a monopole tends to take a stable configuration even in the theories where static solutions are nonexistent. This is true for any initial configuration, which indicates the existence of stationary solutions. While, in the case of  $\lambda/e^2 < 1$ , the dynamics also depends on  $\lambda/e^2$  and initial configuration. In some cases the effect of the gauge fields becomes dominant and a monopole collapses into a black hole.

We should notice that the condition of inflation was also estimated analytically in a simplified model by Tachizawa et al. [3] They discussed the global structure of a space-time by regarding the inside the monopole core as de Sitter spacetime and the outside as

Reissner-Nordström spacetime. They showed that the surface of the monopole core exceeds a cosmological horizon if  $\eta > m_{\text{Pl}}/\sqrt{3\pi} \approx 0.33m_{\text{Pl}}$ . This condition almost agrees with the condition of inflation for most cases in our analysis; this agreement suggests that our numerical results are reasonable as well as that their simplified model is a good approximation in most cases. When the effect of the gauge fields is dominant to that of the Higgs field, however, the spacetime is not de Sitter-like, and then the validity of the simplified model is lost.

Our results as a whole support the discussions of Linde and Vilenkin [5], who pointed out the possibility of monopole inflation. Actually, we have found that inflation happens in most cases of  $\eta > \eta_{\text{cr}}$ . Further, if the initial size of a monopole is large enough, the effect of the gauge fields is not important, as Linde mentioned. What we have clarified more about this subject is there are some cases where static solutions are nonexistent but monopoles do not continue to expand, as the results in Figs. 6 and 7. Although we did not state this fact in our previous paper [6], it is also true for global monopoles.

#### **ACKNOWLEDGMENTS**

The author would like to thank J. Koga, A. Linde, K. Maeda, D. Maison, T. Tachizawa, T. Torii, and A. Vilenkin for useful discussions. Thanks are also due to P. Haines and W. Rozycki for reading the manuscript. This work was supported partially by the Grant-in-Aid for Scientific Research Fund of the Ministry of Education, Science and Culture (No.07740226) and by a Waseda University Grant for Special Research Projects.

## REFERENCES

- [1] P. Breitenlohner, P. Forgàcs, and D. Maison, Nucl. Phys. **B383**, 357 (1992).
- [2] M.E. Ortiz, Phys. Rev. D **45**, R2586 (1992);  
 K. Lee, V.P. Nair, and E.J. Weinberg, *ibid.* **45**, 2751 (1992);  
 P. Breitenlohner, P. Forgàcs, and D. Maison, Nucl. Phys. **B442**, 126 (1995).
- [3] T. Tachizawa, K. Maeda, and T. Torii, Phys. Rev. D **51**, 4054 (1995).
- [4] K. Sato, M. Sasaki, H. Kodama, and K. Maeda, Prog. Theor. Phys. **65**, 1443 (1981);  
 K. Sato, H. Kodama, M. Sasaki, and K. Maeda, Phys. Lett. B **108**, 103 (1982).
- [5] A. Linde, Phys. Lett. B **327**, 208 (1994);  
 A. Linde and D. Linde, Phys. Rev. D **50**, 2456 (1994);  
 A. Vilenkin, Phys. Rev. Lett. **72**, 3137 (1994).
- [6] N. Sakai, H. Shinkai, T. Tachizawa, and K. Maeda, Phys. Rev. D **53** 655 (1996).
- [7] Y. Nambu and M. Siino, Phys. Rev. D **46**, 5367 (1992).

### Figure Captions

**FIG.1.** Configurations of  $\Phi_{\text{flat}}(r)$  and of  $w_{\text{flat}}(r)$  in (2.16), which are adopted as initial conditions for time-evolutions.

**FIG.2.** Dynamics of a monopole for the case of weak gravity. We set  $\eta = 0.1m_{\text{Pl}}$  and  $\lambda/e^2 = 0.1$ , and give two initial configurations:  $c_{\Phi} = c_w = 1$  and 0.5. We plot the trajectories of  $X_{\Phi}(t)$  in (a) and of  $X_w(t)$  in (b). The fields behave stably; these reasonable results indicates that our numerical code works well.

**FIG. 3.** Dynamics of a monopole for  $\eta = 0.4m_{\text{Pl}}$  and  $\lambda/e^2 = 0.1$ . We assume two initial configurations:  $c_{\Phi} = c_w = 1$  in (a) and  $c_{\Phi} = c_w = 10$  in (b). In (a) and (b) we plot the trajectories of  $X_{\Phi}(t)$  and  $X_w(t)$  as well as apparent horizons. In (a) a monopole shrinks and the black-hole horizons appear, while in (b) a cosmological horizon exists from the beginning and a monopole continues to expand. We also draw the distributions of  $\rho + \Sigma p_i$  in (c) and in (d), which correspond the results in (a) and in (b), respectively. In (c) the values around the center get negative at the beginning, but they bounce back to positive values, which confirms that the monopole core never inflates. On the other hand, in (d) the values of  $\rho + \Sigma p_i$  around the center remain negative from the beginning. This behavior indicates that exponential expansion really occurs inside the monopole.

**FIG. 4.** Dynamics of a monopole for  $\eta = 0.55m_{\text{Pl}}$ ,  $\lambda/e^2 = 0.1$  and  $c_\Phi = c_w = 1$ . In (a) we plot the trajectories of  $X_\Phi(t)$  and  $X_w(t)$  as well as apparent horizons. (Please also refer to Fig. 5, which is a schematic sketch of the spacetime structure.) From the beginning there are two apparent horizons,  $S1$  and  $S2$ :  $S1$  is the cosmological horizon. Later other two apparent horizons,  $S3$  and  $S4$ , appear, and then  $S2$  and  $S4$  approach each other. These surfaces turn out to be black-hole horizons,  $S2'$  and  $S4'$ , the moment they intersect. In (b) we draw the distributions of  $\rho + \Sigma p_i$ . The values around the center are initially positive, but they become negative. This suggests that, if  $\eta$  is large enough, a monopole begins to expand exponentially even if its initial size is not so large. We also show in (c) the relation between the proper distance along the radial direction and the circumference radius, which indicates a wormhole structure really appears.

**FIG. 5.** Schematic sketches of the spacetime structure. These figures are not generated from the numerical data, but they are based on the results presented in Fig. 4.

**FIG. 6.** Dynamics of a monopole for  $\eta = 0.3m_{\text{Pl}}$  and  $\lambda/e^2 = 1$ . Setting  $c_\Phi = c_w = 1$ , we show the evolution of  $\Phi$  in (a) and that of  $w$  in (b), and the trajectories of  $X_\Phi(t)$  and of  $X_w(t)$  in (c). Although some oscillations remain outside the monopole, the core of the monopole approaches a stable configuration. We change the initial size in (d), finding monopoles with any initial size behave stably. These results indicate that there exist stationary solutions.

**FIG. 7.** Formation of a monopole from the perturbed symmetric state (de Sitter spacetime). An initial configuration is given by (3.4). We draw the configuration of  $\Phi$  in (a) and that of  $w$  in (b), and the trajectories of  $X_\Phi(t)$  and  $X_w(t)$  in (c). Once a monopole configuration is formed, the monopole approaches a stable configuration instead of continuing to expand. This result supports the existence of stationary solutions.

**FIG. 8.** Parameter plane of  $\eta/m_{\text{Pl}}$  and  $\lambda/e^2$  in which we summarize our numerical results. A square ( $\square$ ) denotes a stable solution, as is the case in Fig. 2 or 6. A cross ( $\times$ ) denotes the case where a monopole shrinks, as is the case in Fig. 3(a). A circle ( $\circ$ ) denotes the case where a monopole inflates and the wormhole structure appears, as is the case in Fig. 3(c) or 4. A dotted line indicates the maximum values of  $\eta/m_{\text{Pl}}$  versus  $\lambda/e^2$ , depicted approximately by use of Fig.6 in [1]. We vary  $c_\Phi$  and  $c_w$  from 1 to 10, and hence some parameter points are labeled as two symbols.

This figure "fig1-1.png" is available in "png" format from:

<http://arxiv.org/ps/gr-qc/9512045v3>

This figure "fig4c-1.png" is available in "png" format from:

<http://arxiv.org/ps/gr-qc/9512045v3>

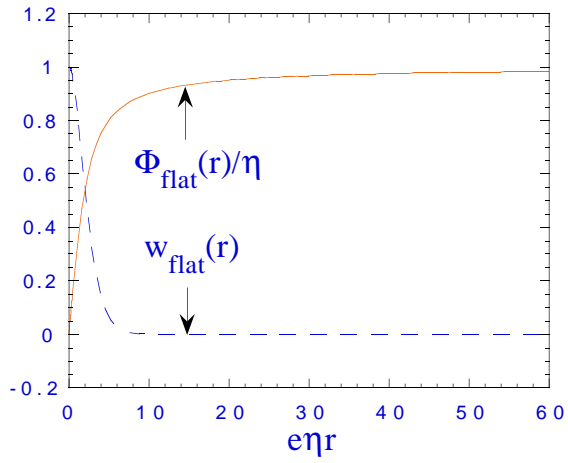


Fig. 1

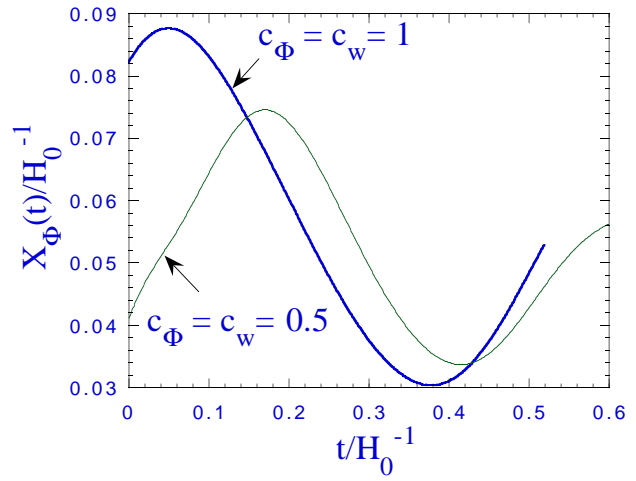


Fig. 2(a)

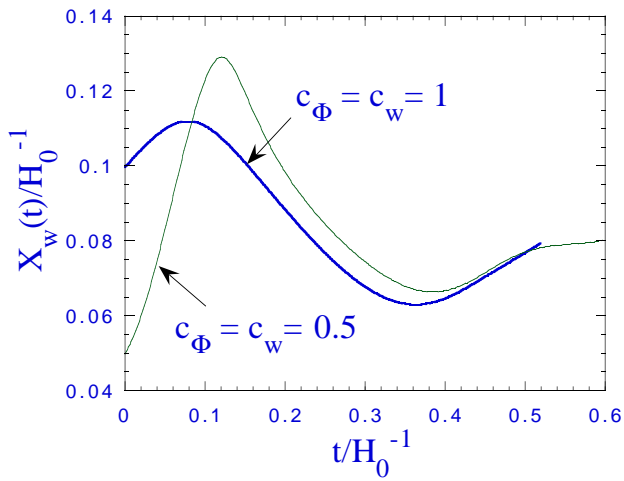


Fig. 2(b)

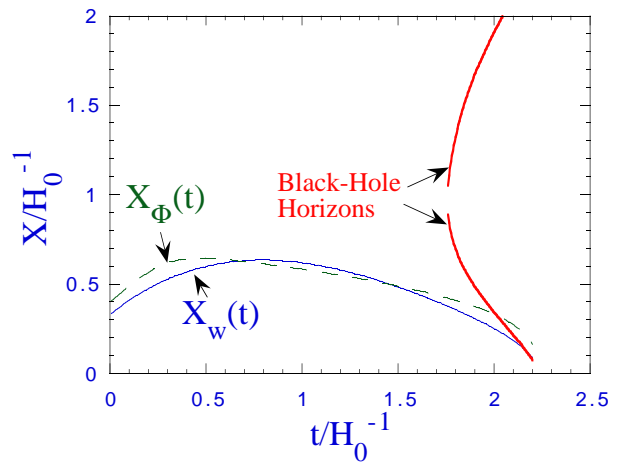


Fig.3(a)

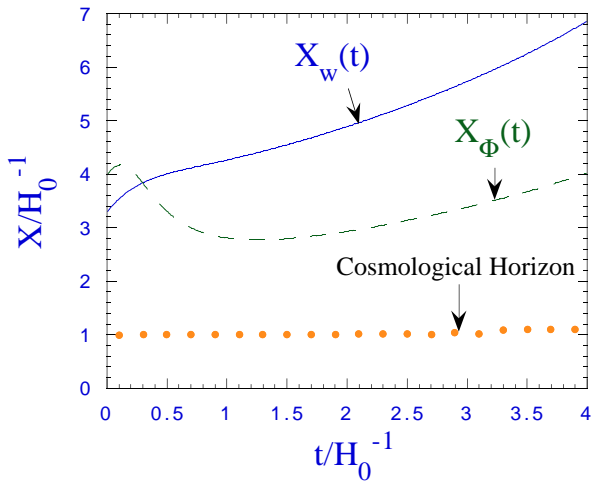


Fig.3(b)

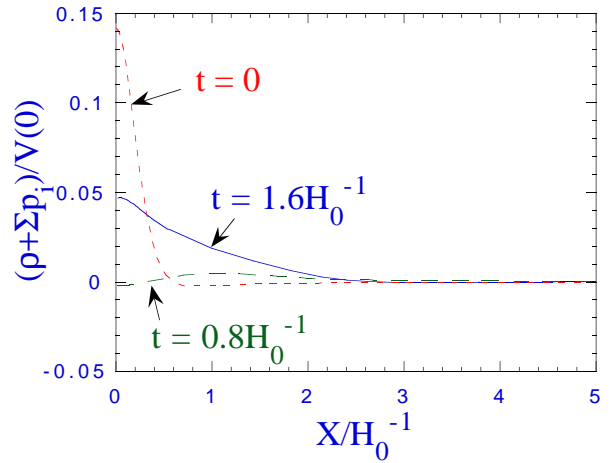


Fig.3(c)

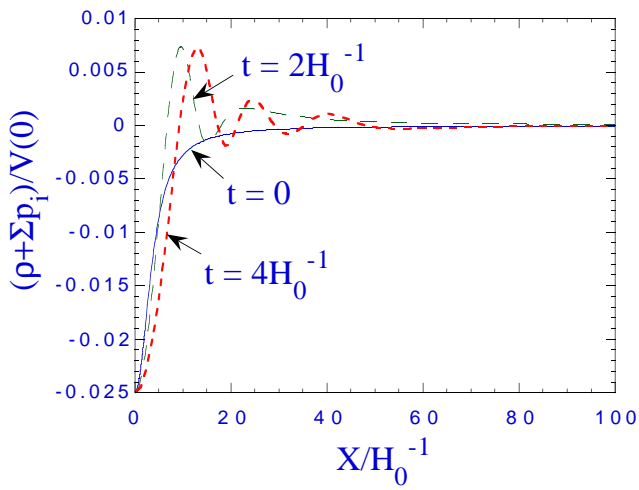


Fig.3(d)

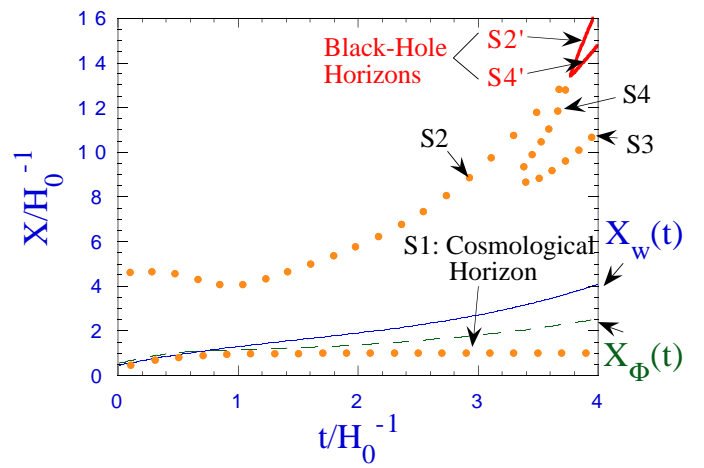


Fig.4(a)

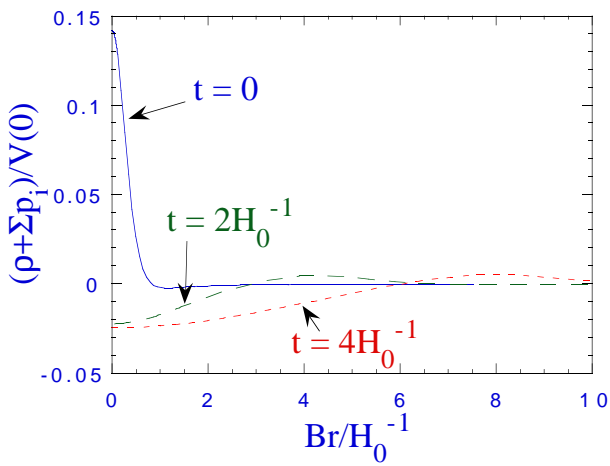


Fig.4(b)

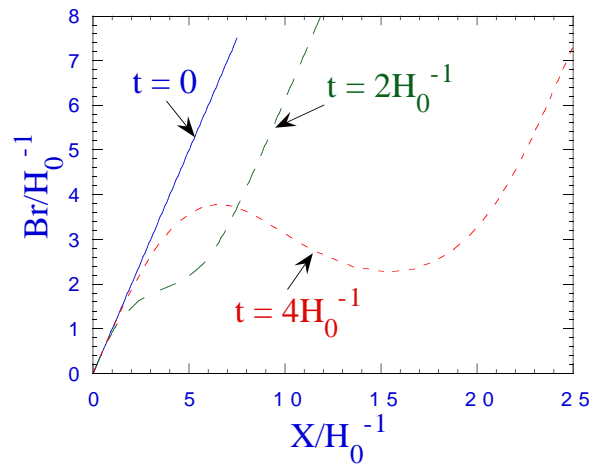


Fig.4(c)

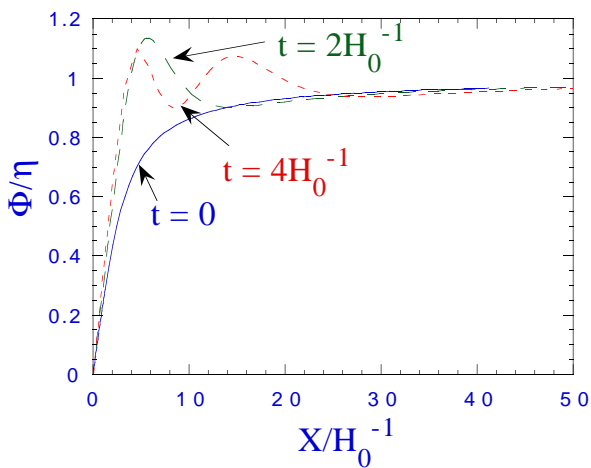


Fig.6(a)

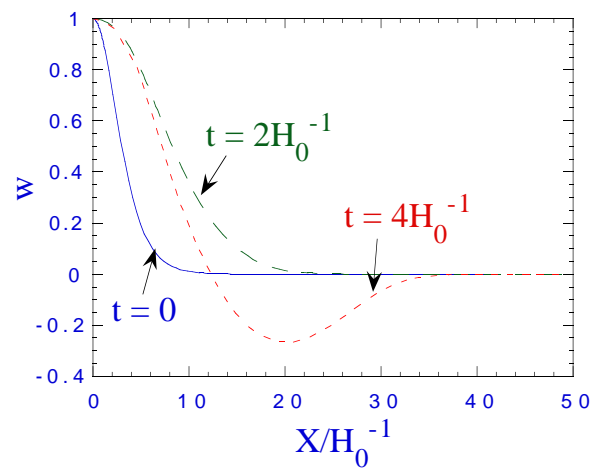


Fig.6(b)

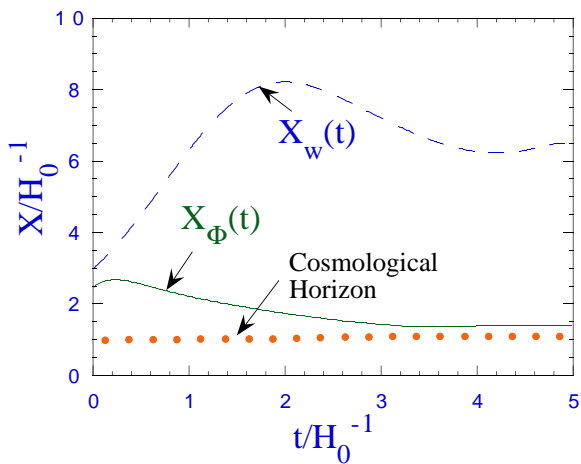


Fig.6(c)

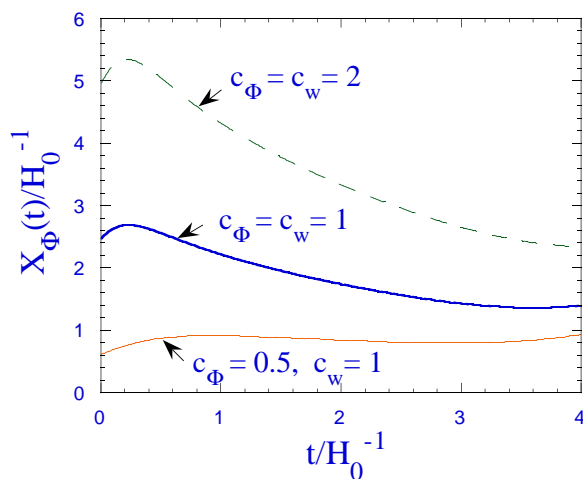


Fig.6(d)

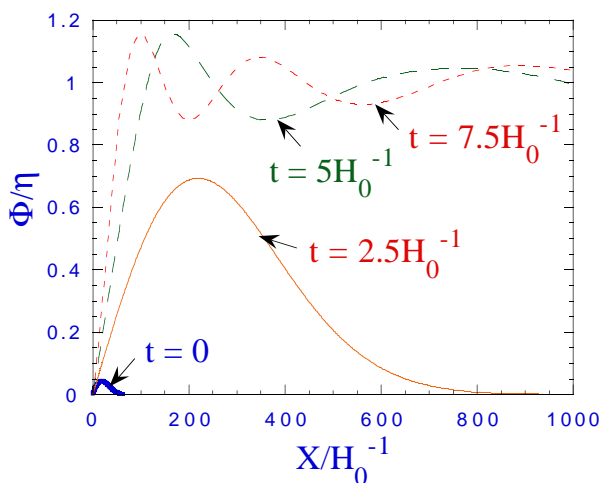


Fig.7(a)

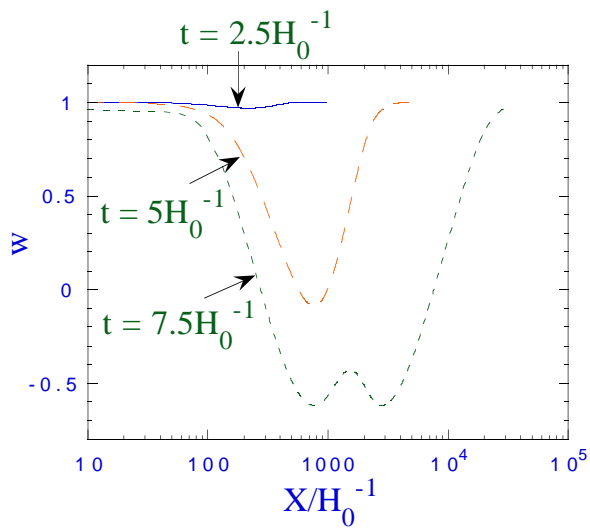


Fig.7(b)

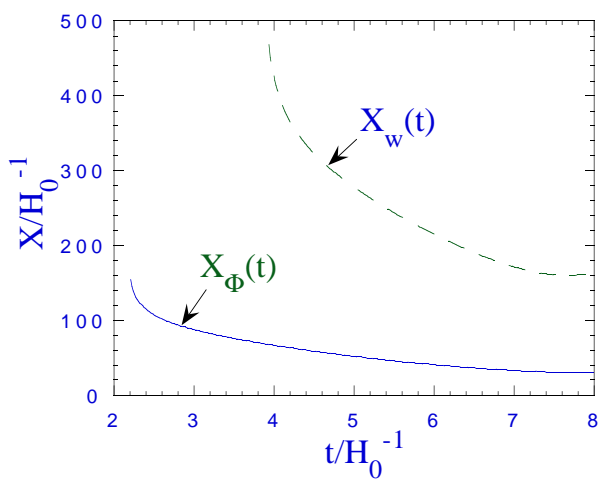


Fig.7(c)

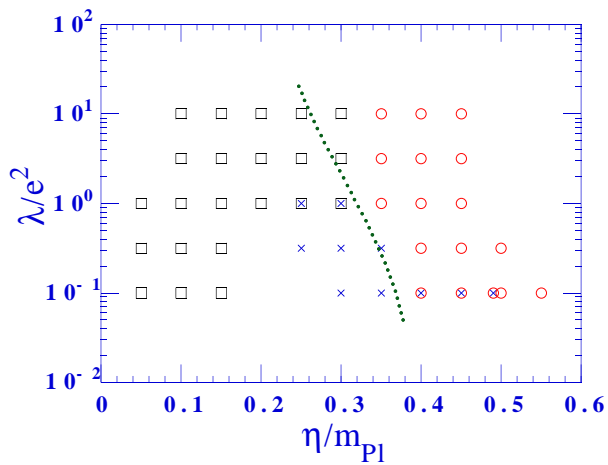


Fig.8